Redox Biology 9 (2016) 90–99

Contents lists available at ScienceDirect

Redox Biology

journal homepage: www.elsevier.com/locate/redox

Research paper

The hydroxypyridinone iron chelator CP94 increases methyl-aminolevulinate-based photodynamic cell killing by increasing the generation of reactive oxygen species

Yuktee Dogra [a,1,2], Daniel C.J. Ferguson [a,2], Nicholas J.F. Dodd [b], Gary R. Smerdon [c], Alison Curnow [d], Paul G. Winyard [a,*]

[a] University of Exeter Medical School, Exeter, Devon EX1 2LU, United Kingdom
[b] University of Plymouth, Drake Circus, Plymouth, Devon PL4 8AA, United Kingdom
[c] DDRC Healthcare, Plymouth Science Park, Research Way, Plymouth, Devon PL6 8BU, United Kingdom
[d] University of Exeter Medical School, Truro, Cornwall TR1 3HD, United Kingdom

ARTICLE INFO

Article history:
Received 12 May 2016
Received in revised form
23 June 2016
Accepted 5 July 2016
Available online 7 July 2016

Keywords:
Apoptosis
Electron paramagnetic resonance (EPR) spectrometry
Necrosis
Photodynamic therapy (PDT)
Protoporphyrin IX (PpIX)
Reactive oxygen species (ROS)
Skin cancer

ABSTRACT

Methyl-aminolevulinate-based photodynamic therapy (MAL-PDT) is utilised clinically for the treatment of non-melanoma skin cancers and pre-cancers and the hydroxypyridinone iron chelator, CP94, has successfully been demonstrated to increase MAL-PDT efficacy in an initial clinical pilot study. However, the biochemical and photochemical processes leading to CP94-enhanced photodynamic cell death, beyond the well-documented increases in accumulation of the photosensitiser protoporphyrin IX (PpIX), have not yet been fully elucidated. This investigation demonstrated that MAL-based photodynamic cell killing of cultured human squamous carcinoma cells (A431) occurred in a predominantly necrotic manner following the generation of singlet oxygen and ROS. Augmenting MAL-based photodynamic cell killing with CP94 co-treatment resulted in increased PpIX accumulation, MitoSOX-detectable ROS generation (probably of mitochondrial origin) and necrotic cell death, but did not affect singlet oxygen generation. We also report (to our knowledge, for the first time) the detection of intracellular PpIX-generated singlet oxygen in whole cells via electron paramagnetic resonance spectroscopy in conjunction with a spin trap.

1. Introduction

Photodynamic therapy (PDT) is a relatively selective way to ablate diseased cells, particularly tumours, without harming normal surrounding tissues [1]. Successful PDT involves three key components; pre-administration of a photosensitising agent, delivery of light of a specific wavelength as well as the presence of molecular oxygen [1]. Following photosensitiser accumulation, and assuming sufficient oxygen levels are present, irradiation of the target tissue with the activating light leads to the production of reactive oxygen species (ROS) via Type I and II photochemical reactions [2]. The production of these reactive species leads to cellular damage and thus, if produced in sufficient quantities, cell death [1].

PDT has many applications, including the treatment of bladder, oesophageal and lung cancers, head and neck lesions and brain tumours [3,4]. PDT is most commonly used in dermatology to treat non-melanoma skin cancers and pre-cancers [4]. In dermatological PDT, one of the most commonly used drugs is methyl-aminolevulinate (MAL; Metvix®). As a pro-drug, MAL is enzymatically converted into the naturally occurring photosensitiser, protoporphyrin IX (PpIX), via the haem biosynthesis pathway [5]. An advantage of using MAL over other non-PpIX inducing photosensitive agents is that it is metabolised quickly, decreasing the risk of prolonged cutaneous photosensitivity that can be associated with other classes of photosensitisers. Furthermore, MAL is also topically available (being well absorbed into the skin when applied as a cream formulation) making it a convenient

Abbreviations: A431, Human squamous carcinoma cells; ALA, Aminolaevulinic acid; CP94, 1,2-diethyl-3-hydroxypyridin-4-one; DEPMPO, 5-(diethoxyphosphoryl)-5-methyl-1-pyrroline-N-oxide; DTPA, Diethylenetriaminepentaacetic acid; EPR, Electron paramagnetic resonance; FCS, Fetal calf serum; MAL, Methyl-aminolevulinate; MnTBAP, [5,10,15,20-tetrakis(4-carboxyphenyl)-porphyrinato] manganese(III) chloride; $^1O_2$, Singlet oxygen; O_2, Superoxide; OH, Hydroxyl radical; PpIX, Protoporphyrin IX; PMA, Phorbol myristate acetate; ROS, Reactive oxygen species; SOD, Superoxide dismutase; TEMPOL, 4-hydroxy-2,2,6,6-tetramethylpiperidine-1-oxyl; TMP, 4-hydroxy-2,2,6,6-tetramethylpiperidine

* Corresponding author.
E-mail address: p.g.winyard@exeter.ac.uk (P.G. Winyard).
[1] Present address: College of Life and Environmental Sciences, University of Exeter, Exeter, Devon EX4 4QJ, United Kingdom.
[2] These authors contributed equally to this work.

http://dx.doi.org/10.1016/j.redox.2016.07.002
2213-2317/

photosensitising agent for dermatological PDT applications.

The mechanism of cell death induced by MAL-based PDT is not fully understood. For example, whether cells die primarily through necrosis or apoptosis and over what time period this occurs has not been clearly established. Furthermore, in the cell culture models which are employed to study cell death induced by photoirradiation, the observed effects on cell death are dependent on the protocol and cell type [1]. The generation of ROS during photoirradiation of a photosensitiser occurs via Type I and Type II photochemical reactions [6]. In a biological system, Type I photochemical reactions lead to the production of superoxide anion radicals ($O_2^{\bullet -}$), hydrogen peroxide (H_2O_2) and hydroxyl radicals ($OH^{\bullet}$), while Type II photochemical reactions lead to the production of singlet oxygen ($^1O_2$) [1,7–10]. It is well established that the generation of ROS and $^1O_2$ during photoirradiation of a photosensitiser leads to cellular damage and the initiation of biological cascades which eventually lead to cell death [11,12].

Due to their short lifetimes, the direct measurement of ROS and free radicals is difficult [13]. Fluorogenic probes are frequently utilised in an attempt to detect and quantify ROS generated in many different biological systems. However, these probes are rarely specific and are often used improperly, leading to the detection of multiple ROS with no way to determine which species have been detected [14]. Some methods are capable of improving the specificity of fluorogenic probes. For example, the detection of $O_2^{\bullet -}$ by hydroethidine can be performed by selectively exciting the $O_2^{\bullet -}$-specific product, 2-hydroxyethidium [15]. Despite these improvements, however, electron paramagnetic resonance (EPR) spectroscopy is considered the gold standard for detecting ROS directly and specifically [16–19]. Typically, a nitrone or nitroso compound is used to "trap" a free radical, producing a nitroxide (radical or spin adduct), which possesses stability considerably greater than that of the parent free radical [16,20,21]. Although there have been numerous studies in which EPR has been utilised to detect $^1O_2$ and ROS generated by photosensitisers in a cell-free system [22–27], there appear to be no reports of the same techniques being used to detect ROS generated by photo-irradiated PpIX in whole cells.

Attempts to improve PpIX-based PDT have included the use of iron chelating agents [28]. By chelating free iron, the insertion of iron into the porphyrin ring of PpIX by ferrochelatase is inhibited, which in turn leads to increased prodrug-induced PpIX accumulation [29]. The hydroxypyridinone iron chelator, CP94, has also been used to increase PpIX accumulation within human skin cancers, leading to significant decreases in tumour size following irradiation [30,31]. Although CP94 has shown success as an enhancer of PpIX-induced PDT, the biochemical and photochemical processes behind this effect have not yet been fully elucidated.

In this study, the effects of CP94 on the generation of $^1O_2$ and ROS in A431 human epidermoid squamous carcinoma cells treated with MAL and light have been investigated using EPR spectrometry and the fluorogenic probes dihydroethidium and a mitochondria-targeted derivative, MitoSOX. The results reported here suggest that the increased efficacy of MAL-based photodynamic cell killing performed in conjunction with CP94 iron chelation is, at least in part, due to an increased generation of ROS, likely localised to the mitochondria.

2. Materials and methods

2.1. Chemicals and cells

All reagents were purchased from Sigma-Aldrich Chemical Company (Poole, UK) unless otherwise stated. A431 (human epidermoid squamous carcinoma) cells were purchased from the European Collection of Cell Culture (Wiltshire, UK). Under aseptic conditions in a class II laminar flow cabinet, cells were cultured in DMEM with 10% (v/v) fetal calf serum, 2% (200 mM) L-glutamine (Lonza; Wokingham, UK), 2% penicillin (200 U/ml) and streptomycin (200 μg/ml) solution. Cells were grown in 5% CO_2 at 37 °C and left to grow until 70–80% confluent, at which time the cells were passaged (every 4–5 days).

2.2. Cell treatment and irradiation

Cells were seeded in to T 12.5 cm^2 culture flasks (Scientific Laboratory Supplies; Nottingham, UK) at a concentration of 5×10^5 cells per ml (1×10^6 per flask) and left to grow in 5% CO_2 at 37 °C until they had reached 80% confluence. The medium was aspirated and cells were washed with PBS prior to the addition of test solutions. Test solutions containing MAL (500 μM) ± CP94 (150 μM), MnTBAP (100 μM) or L-histidine (25 mM) were prepared in DMEM growth media and treatments were carried out for 3 h in 5% CO_2 at 37 °C. Following treatment with MAL, all further experimentation was carried out under reduced light conditions to reduce PpIX photobleaching. Irradiation of cells was carried out using a filtered narrow band (630 ± 15 nm) Aktilite CL16 LED array lamp (Galderma, Bath, UK). At room temperature, each flask was inverted and irradiated from above, with the light source 10 cm away from the cells for 5 min to provide a total dose of 25 J/cm^2. Following irradiation, the test solutions were aspirated and fresh DMEM growth media was applied and the cells were returned to the incubator (5% CO_2; 37 °C).

As a positive control for apoptosis, A431 cells seeded in T 12.5 cm^2 flasks were treated with 30 μM etoposide for 20 h. Etoposide is a topoisomerase inhibitor which is well-documented to induce apoptosis [32].

2.3. Assessment of cell death

Cell death was assessed using annexin V-FITC and propidium iodide in conjunction with a Beckman Coulter Quanta SC flow cytometer. The data collected were analysed using Cell Lab Quanta™ software (Beckman Coulter, High Wycombe, UK). Cells that were only stained with propidium iodide were designated "necrotic". Cells that were stained with annexin V-FITC, with or without propidium iodide staining, were designated "apoptotic". For the time course, cell death was assessed at 0, 2, 4, 8, 16 and 20 h post-irradiation. When examining the effects of MnTBAP and L-histidine, cell death was assessed at 20 h post-irradiation. Cells were trypsinised, washed twice with PBS and re-suspended in 100 μl ice cold calcium buffer (140 mM NaCl, 4 mM KCl, 0.75 mM $MgCl_2$, 1.5 mM $CaCl_2$ and 10 mM HEPES) containing 1.25 μg/ml annexin V-FITC. After 15 min incubation on ice in the dark, 900 μl of Ca^{2+} buffer containing 0.04 mg/ml propidium iodide was added to the cell suspension ready for analysis by flow cytometry.

2.4. Protoporphyrin IX fluorescence measurements

Cells were seeded into a 96 well plate at a concentration of 1×10^5 per ml (2×10^4 per well) and left to adhere overnight in 5% CO_2 at 37 °C. The medium was aspirated and cells were washed with PBS (Lonza) prior to the addition of test solutions. A range of concentrations of MAL (0–2000 μM) ± 150 μM CP94 were prepared in DMEM growth media in reduced light levels. Each concentration was tested in triplicate in a minimum of 6 separate experiments. After 3 h of treatment in 5% CO_2 at 37 °C, cells were washed with PBS twice, after which 100 μl of PBS was added to each well and protoporphyrin IX fluorescence was measured using a Pherastar fluorescence plate reader (BMG Labtech; Aylesbury, UK), utilising a 410 nm excitation wavelength and 630 nm

emission wavelength. A standard curve of pre-synthesised PpIX (0–2 μM) was also prepared and measured in each plate, allowing for interpolation of a PpIX concentration.

2.5. Detecting ROS using dihydroethidium

A431 cells were seeded and treated as described above. One hour prior to irradiation, DHE or MitoSOX was added to each flask at a final concentration of 10 μM or 2.5 μM, respectively. Following irradiation, each flask was prepared immediately for analysis by flow cytometry: the cells were trypsinised, washed and suspended in 1 ml of cold PBS ready for analysis. The fluorescence emission of the superoxide-specific oxidation products, 2-OH-E^+ and Mito-2-OH-E^+, excited with a filtered xenon lamp (370 ± 30 nm) and emission was monitored at 575 ± 10 nm. This method was adapted from Robinson et al., as a means of detecting the superoxide-specific reaction product [15]. As a positive control for DHE and MitoSOX detection of $O_2^{\bullet -}$ in our system, A431 cells were treated with carbonyl cyanide *m*-chlorophenylhydrazone (CCCP). Cells were treated with 10 μM CCCP for 2 h, after which 10 μM of DHE or 2.5 μM of MitoSOX was added for 1 h. Cells were prepared for flow cytometry and analysed as described above.

2.6. Neutrophil separation

Peripheral blood was collected from healthy human volunteers in 15 ml vacutainer tubes containing 1.5 mg/ml EDTA (Becton-Dickinson UK Ltd.; Oxford, UK). The blood was layered over Polymorphprep™ (Axis-Shield; Oslo, Norway) in a 15 ml tube and centrifuged at $500 \times g$ for 35 min. The neutrophil layer was removed using a fine-tipped pipette and then diluted in 0.45% (w/v) NaCl and centrifuged at $200 \times g$ for 5 min. The supernatant was discarded and the pelleted neutrophils were re-suspended in 5 ml of water, lysing any contaminating red blood cells, before 5 ml of 0.9% NaCl solution was added to restore osmolality. This step was repeated until any red blood cell contamination that existed was removed.

2.7. EPR spectrometry

The EPR spectra of known concentrations of TEMPOL (Axxora Ltd; Birmingham, UK) were obtained, in order to establish a concentration-signal response relationship in our system. By plotting the area under the curve for each spectrum against the concentration of TEMPOL (0–5 μM), a standard curve was produced with a linear regression coefficient of > 0.98 (data not shown).

The spin traps used in this investigation were 4-hydroxy-2,2,6,6-tetramethylpiperidine (TMP; $^1O_2$ trap) and 5-(diethoxyphosphoryl)-5-methyl-1-pyrroline-N-oxide (DEPMPO; $O_2^{\bullet -}$ trap). Prior to experimentation it was necessary to set up a positive control for both of the spin traps.

As a positive control for DEPMPO trapping of $O_2^{\bullet -}$, isolated human neutrophils were treated with phorbol myristate acetate (PMA), causing a NADPH-dependent burst of $O_2^{\bullet -}$ [33,34] which, in the presence of DEPMPO, leads to the formation of the spin adduct DEPMPO-OOH. This protocol was adapted from Roubaud et al. [35]: once the neutrophils had been washed, they were suspended in 1 ml of PBS (4×10^6 cells/ml) containing glucose (1 mg/ml), albumin (1 mg/ml) and DTPA (0.1 mM) and stored on ice until used. PMA (in PBS, 200 ng/ml) was added to the cell suspension along with DEPMPO (20 mM in PBS) in the absence or presence of bovine superoxide dismutase (SOD) (400 U/ml). EPR spectra were acquired at room temperature using a RE1X EPR spectrometer (Jeol Ltd., Welwyn Garden City, UK). Each sample was injected into a Jeol quartz WG-LC-11 flat cell and placed into the EPR spectrometer prior to spectral acquisition. Acquisitions were carried out at t=0 min, immediately after the addition of PMA, and t =30 min. The spectral acquisition parameters were: microwave frequency: 9.45 GHz, microwave power 10 mW, centre field 3362 G, sweep width 150 G, sweep time 100 s, time constant 0.3 s, modulation frequency 100 kHz, modulation width 0.63 G and average of 3 sweeps.

Pre-synthesised PpIX was irradiated (630 nm) in the presence of TMP as a positive control for TMP trapping of $^1O_2$. TMP was prepared in 100% methanol and diluted in PBS to a final concentration of 100 mM and pre-synthesised PpIX (20 μM) was prepared in DMSO. PpIX and TMP were mixed in a 1:1 ratio, giving final concentrations of 50 mM TMP and 10 μM PpIX, injected into the flat cell and placed in the EPR cavity. A spectrum was acquired immediately, in the absence of photo-irradiation. The sample was then irradiated through the irradiation window in the EPR cavity for 5 min (25 J/cm^2) by an Aktilite CL16-LED lamp, after which a second spectrum was acquired. The spectral acquisition parameters were microwave frequency 9.45 GHz, microwave power 4 mW, centre field 3360 G, sweep width 50 G, sweep time 100 s, time constant 1 s, modulation frequency 100 kHz, modulation width 1.25 G and average of 3 sweeps.

Measurements of $^1O_2$ and $O_2^{\bullet -}$ generated in A431 cells during irradiation were carried out following treatment with MAL ± CP94 as previously described. After 2.5 h of treatment, cells were also treated with either TMP (50 mM) or DEPMPO (20 mM) for 30 min. Following treatment, the cells were trypsinised, washed and suspended in PBS to a density of 1×10^6 cells/ml prior to injection into the flat cell. Spectral acquisitions were then carried out as before, with acquisitions pre- and post-irradiation.

3. Results

3.1. MAL-based photodynamic cell killing

Each treatment group (untreated, treatment with MAL and irradiation, and treatment with MAL, CP94 and irradiation) exhibited low amounts of apoptosis (2–3%) at each time point measured (0–20 h, Fig. 1A), with no statistically significant difference in the extent of apoptosis between each of the treatments, nor between any of the time points ($p > 0.05$, Kruskal-Wallis test). In contrast, at 20 h, cells treated with the known pro-apoptotic compound, etoposide, showed $34.2 \pm 5.5\%$ (mean ± SD) apoptosis and $6.4 \pm 1.3\%$ necrosis.

Untreated cells exhibited low amounts of necrosis at each time point measured, with no significant change over the time course of the experiment (Fig. 1A). When A431 cells were treated with MAL and irradiation, a time-dependent increase in necrosis was observed, with ~9% necrosis at 4 h post-irradiation, $14.2 \pm 1.6\%$, at 8 h and $22.5 \pm 1.1\%$ at 20 h.

Following treatment with MAL, CP94 and irradiation, the percentage of necrosis increased 2 h post-irradiation ($11.1 \pm 0.9\%$) and continued to increase at 4 h ($15.5 \pm 0.7\%$), 8 h ($18.7 \pm 0.9\%$), 16 h ($31.4 \pm 1.7\%$) and 20 h ($42.3 \pm 2.4\%$). At each time point, the percentage of necrosis was found to be significantly increased over that of the MAL and irradiation treatment ($p < 0.05$, Kruskal-Wallis test).

3.2. Effects of CP94 on MAL-induced PpIX accumulation in A431 cells

The treatment of A431 cells with MAL resulted in the accumulation of PpIX in a concentration-dependent manner (Fig. 2). The accumulation of PpIX was significantly increased when cells were concurrently treated with MAL (0.4, 0.5, 1 and 2 mM, $p < 0.001$) and 150 μM CP94 compared with the corresponding concentration of MAL alone. When treated with MAL-only (2 mM),

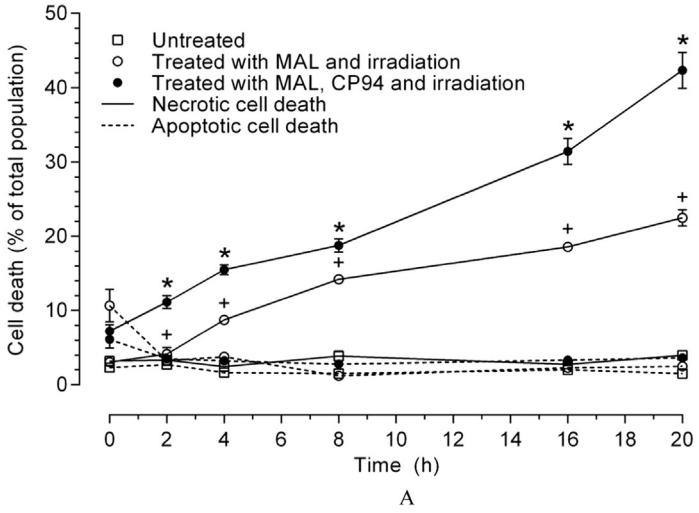

A

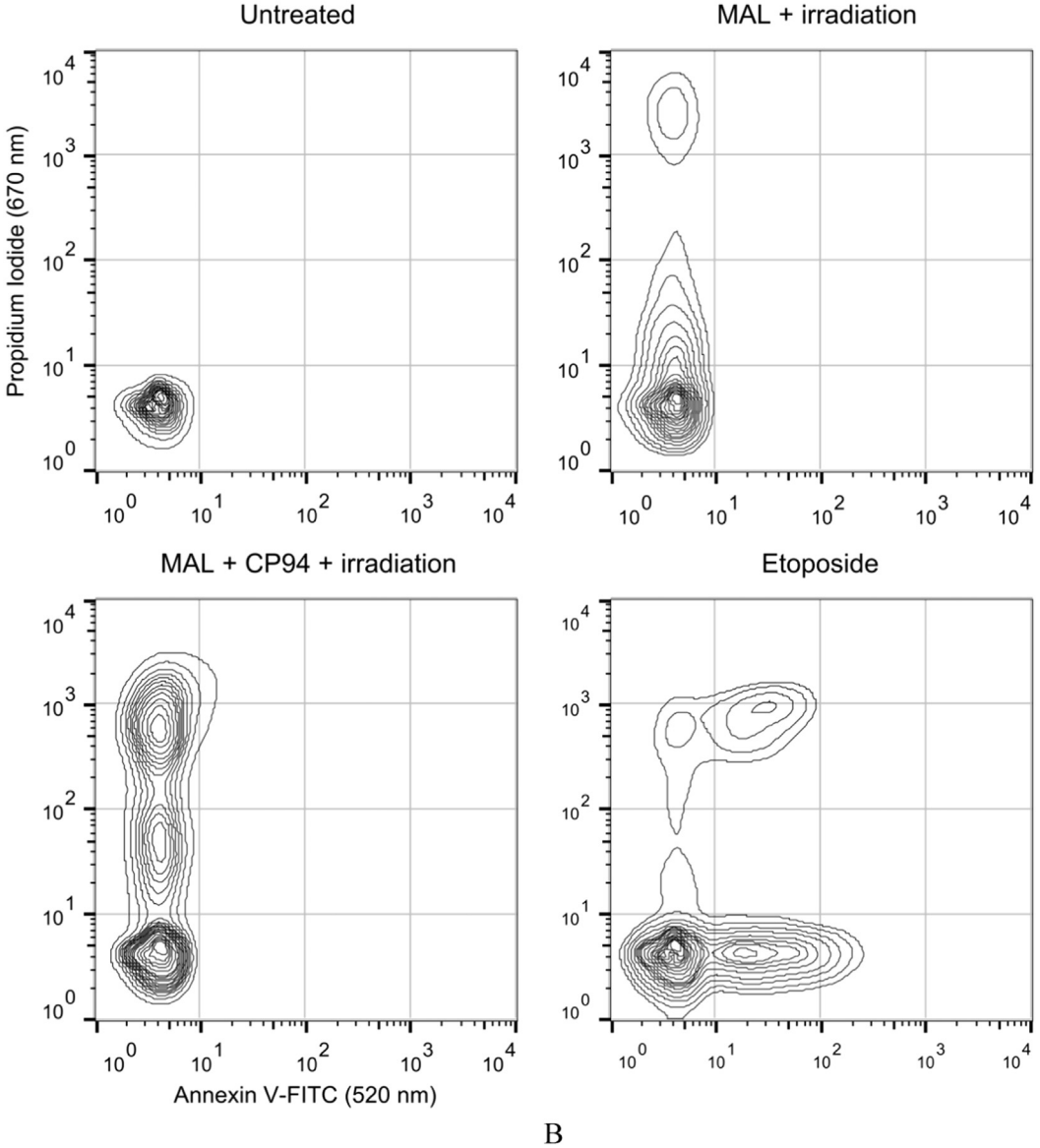

B

Fig. 1. (A) Time-course of cell death induced by MAL (0.5 mM) and irradiation (25 J/cm^2) in the absence and presence of CP94 (150 μM) within the A431 cells. The graphs show the effect of treatment on apoptosis (dashed lines) and necrosis (solid lines), as indicated by annexin V-FITC and propidium iodide staining. Analysis was carried out on untreated cells (open squares), cells treated with MAL and irradiation (open circles) and MAL, CP94 and irradiation (closed circles). Cells were assessed post-irradiation by flow cytometry. The data are presented as mean ± one standard deviation, n=9. + corresponds to $p < 0.05$ (Kruskal-Wallis test), comparing untreated cells to cells treated with a combination of MAL and irradiation and * corresponds to $p < 0.05$ comparing untreated cells to cells treated with a combination of MAL, CP94 and irradiation, at each given time point. (B) Representative contour plots and histograms showing annexin V-FITC and propidium iodide staining of A431 cells following photodynamic cell killing.

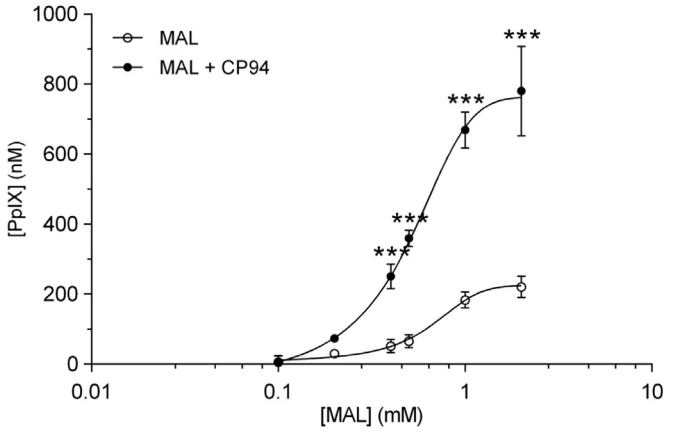

Fig. 2. Concentration-response curves showing the effects of MAL ± CP94 on PpIX accumulation. A431 cells were treated with 0 – 2 mM MAL (open circles) ± 150 μM CP94 (closed circles) for 3 h, after which PpIX fluorescence was measured (ex: λ_{max} 410 nm, em: λ_{max} 630 nm) and total concentration was interpolated using a standard curve. Results were normalised by subtracting data for 0 mM MAL from all data points. Data presented as mean ± one standard deviation, n=6. *** corresponds to $p < 0.001$ Student's *t*-test compared to cells treated with MAL.

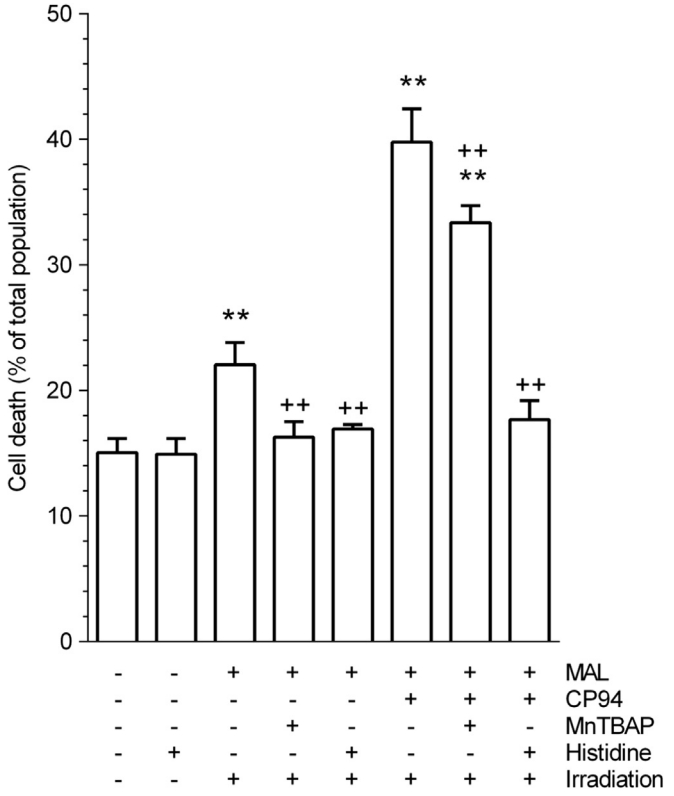

Fig. 3. Effects of MnTBAP and L-histidine on photodynamic cell killing. A431 cells were treated with MAL (0.5 mM) ± CP94 (150 μM) and MnTBAP (100 μM) or L-histidine (25 mM) for 3 h. Following this, cells were irradiated (25 J/cm^2) and cell death was assessed 20 h post-irradiation by annexin V-FITC and propidium iodide staining in conjunction with flow cytometry. Data are presented as the mean of total cell death ± one standard deviation, n=6. ** corresponds to $p < 0.01$, Student's *t*-test compared to untreated (control) cells. ++ corresponds to $p < 0.001$ compared to cells treated in the absence of MnTBAP or L-histidine.

PpIX accumulation peaked at ~200 nM. The addition of CP94 increased peak PpIX accumulation four-fold to 800 nM ($p < 0.001$).

3.3. Effects of MnTBAP and L-histidine on photodynamic cell killing

Total cell death was assessed 20 h after photodynamic treatment in the absence and presence of the SOD-mimetic MnTBAP, or the singlet oxygen quencher L-histidine (Fig 3.). Background cell death (untreated cells) was 15.5 ± 0.5% (mean ± SD). Following treatment with MAL and irradiation, cell death increased to 22.1 ± 1.8% ($p < 0.01$ compared to untreated) and this increased further to 39.8 ± 2.6% in cells also treated with CP94 ($p < 0.01$ compared to treatment with MAL and irradiation). Co-treatment with MnTBAP or L-histidine completely protected cells from photodynamic cell killing by treatment with the combination of MAL and irradiation (16.3 ± 1.2% and 16.9 ± 0.4% respectively, $p < 0.01$) which was not significantly different from untreated cells ($p = 0.2$). MnTBAP and L-histidine also significantly decreased killing of cells treated with MAL, CP94 and irradiation. Under these conditions, MnTBAP partially protected cells from photodynamic cell killing (33.4 ± 1.3%, $p < 0.01$) whilst L-histidine completely protected cells (17.7 ± 1.5%, $p < 0.01$). The high concentration of L-histidine (25 mM) used here was found to have no effect on cell viability when added alone (14.9 ± 1.2% cell death).

3.4. Dihydroethidium and MitoSOX detection of ROS generated in cells exposed to MAL-based photodynamic cell killing

DHE and a mitochondria-targeted derivative, MitoSOX, were used to assess the generation of cytosolic and mitochondria-localised ROS by PpIX following irradiation. The results, presented in Fig. 4A and B, are displayed as a percentage of 2-OH-E$^+$ fluorescence detected in untreated (i.e. control) cells (DHE: 100.0 ± 2.8%, MitoSOX: 100 ± 3.4%). Cells treated with CCCP as a positive control exhibited a significant increase in fluorescence (DHE: 154.9 ± 11.7%, MitoSOX: 142.5 ± 5.0%, $p < 0.01$ compared to untreated, data not shown). Compared to untreated controls, treatment with MnTBAP alone significantly decreased both DHE fluorescence (90.6 ± 3.1%) and MitoSOX fluorescence (41.6 ± 1.4%; $p < 0.01$).

Cells which underwent treatment with MAL and irradiation also exhibited a significant increase in fluorescence (DHE: 156.6 ± 8.5%, MitoSOX: 192.4 ± 12.5%, $p < 0.001$ compared to untreated) and this increased further in cells which were also treated with CP94 (DHE: 197.3 11.3%, MitoSOX: 405.3 ± 11.5%, $p < 0.001$ compared to treatment with MAL and irradiation).

Addition of the SOD-mimetic MnTBAP to all treatments resulted in significant decreases in fluorescence. Cells treated with MAL and irradiation in the presence of MnTBAP exhibited DHE and MitoSOX fluorescence at 50.5 ± 0.6% and 69.6 ± 6.8% of the mean level observed in the untreated (control) cells ($p < 0.001$ compared to treatment with MAL and irradiation). The cells which were treated with MAL, CP94 and irradiation in the presence of MnTBAP exhibited fluorescence of 33.4 ± 5.9% and 136.6 ± 3.0% ($p < 0.01$ compared to treatment with MAL, CP94 and irradiation).

3.5. EPR detection of ROS generated in cells exposed to MAL-based photodynamic cell killing

When neutrophils (4×10^6 cells/ml) were stimulated by PMA in the presence of DEPMPO, the EPR signal observed was that of the $O_2^{\bullet -}$ adduct (Fig. 5B), DEPMPO-OOH, with hyperfine splitting of: $a^N = 13.4$ G, $a^{H\beta} = 11.9$ G, $a^{H\gamma} = 0.8$ (1 h), 0.43 (6 h) and $a^P = 52.5$ G. The presence of DTPA prevented the formation of the transition metal-dependent hydroxyl radical formation, ensuring that the DEPMPO hydroxyl radical adduct was not formed. In the absence of PMA, no signal was observed (Fig. 5A) and the addition of active SOD to PMA-treated neutrophils suppressed the signal completely (Fig. 5C). When cells were treated with MAL ± CP94, no DEPMPO-OOH adduct was detected pre- or post-irradiation (Fig. 5D and E).

Singlet oxygen reacts with the spin trap TMP to form the stable nitroxide free radical 4-hydroxy-2,2,6,6-tetramethylpiperidinyloxy

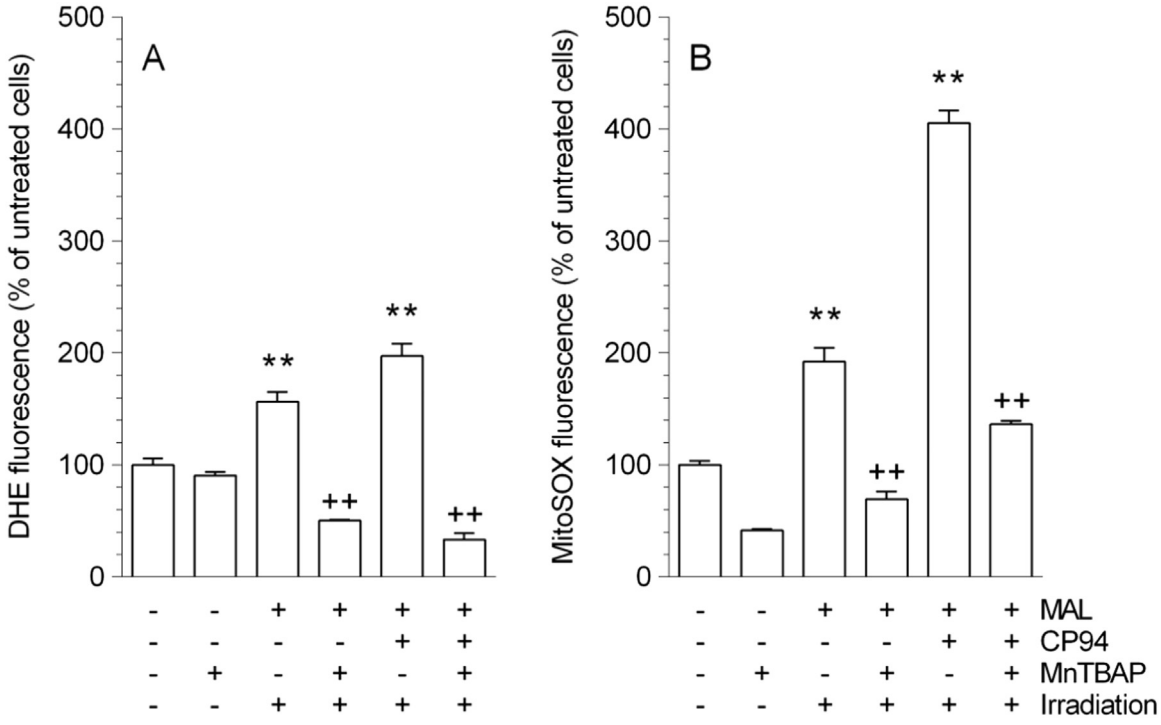

Fig. 4. Effects of MnTBAP on photo-generated ROS as detected by DHE or MitoSOX. A431 cells were treated with MAL (0.5 mM) ± CP94 (150 μM) and MnTBAP (100 μM) for 3 h. After 2 h, cells were treated with (A) 10 μM DHE or (B) 2.5 μM MitoSOX for 1 h. Following this, cells were irradiated (25 J/cm^2) and immediately analysed by flow cytometry. Data are presented as the mean ± one standard deviation, n = 6. ** corresponds to $p < 0.01$, Student's *t*-test compared to untreated (control) cells. ++ corresponds to $p < 0.001$ compared to cells treated in the absence of MnTBAP. (A) 100% = 120.73 RFU, (B) 100% = 100.09 RFU.

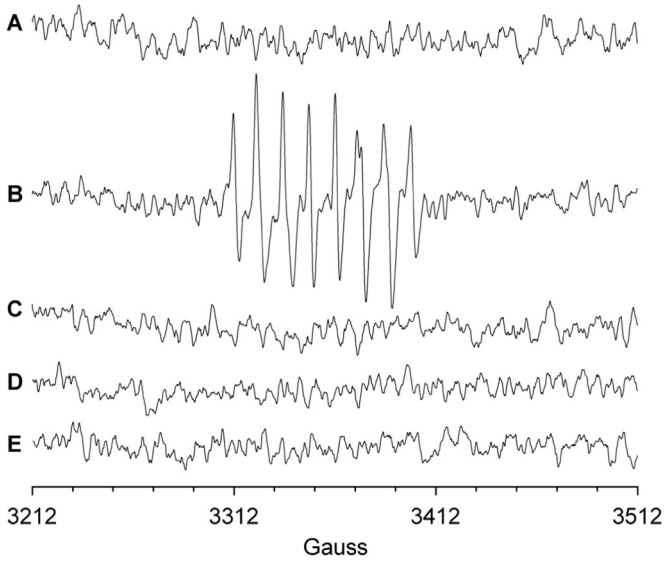

Fig. 5. EPR spectra obtained from (A) un-stimulated neutrophils after 30 min, (B) stimulated neutrophils 30 min after the addition of PMA (200 ng/ml) and (C) stimulated neutrophils in the presence of SOD (400 U/ml), 30 min after the addition of PMA. A431 cells were treated with MAL (0.5 mM) and CP94 (150 μM) and spectra were acquired (D) pre-irradiation (E) and post-irradiation (25 J/cm^2). Each spectrum is representative of 4 repeat experiments. DEPMPO was added to each condition at a concentration of 20 mM. The spectral acquisition parameters were: microwave frequency: 9.45 GHz, microwave power 10 mW, centre field 3362 G, sweep width 150 G, sweep time 100 s, time constant 0.3 s, modulation frequency 100 kHz, modulation width 0.63 G and average of 3 sweeps.

(TEMPOL), which has hyperfine splitting of $a^N = 16.3$ G [36,37]. When pre-synthesised PpIX and TMP were mixed together in the absence of irradiation, a very small background signal from the spin trap was detected (Fig. 6A). However, when the sample was irradiated the signal increased dramatically (Fig. 6B). The

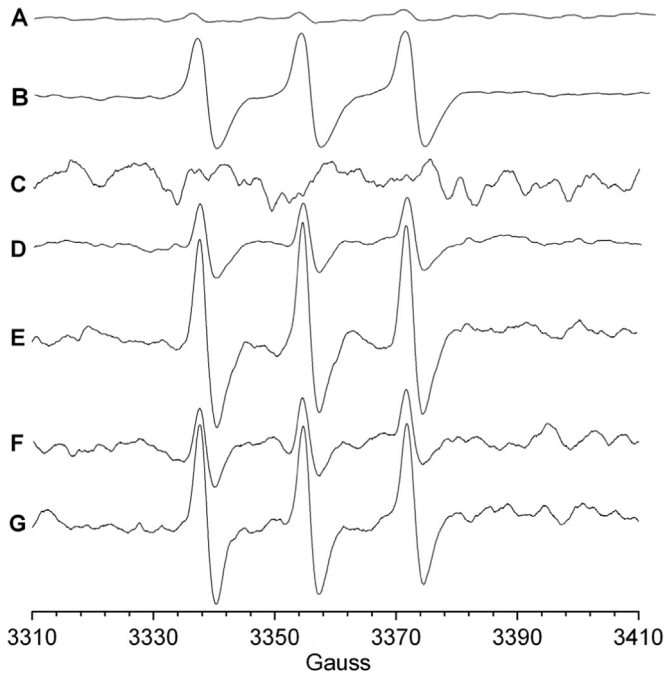

Fig. 6. EPR spectra were acquired from pre-synthesised PpIX (10 μM) and TMP (A) pre-irradiation and (B) post-irradiation (25 J/cm^2). Spectrum (C) is representative of A431 cells treated with TMP only. A431 cells were treated with MAL (0.5 mM) and spectra were acquired (D) pre-irradiation and (E) post-irradiation. A431 cells were also treated with MAL and CP94 (150 μM) and spectra were acquired (F) pre-irradiation and (G) post-irradiation. Each spectrum is representative of 3 repeat experiments. TMP was added to each condition at a concentration of 50 mM. The spectral acquisition parameters were microwave frequency 9.45 GHz, microwave power 4 mW, centre field 3360 G, sweep width 50 G, sweep time 100 s, time constant 1 s, modulation frequency 100 kHz, modulation width 1.25 G and average of 3 sweeps.

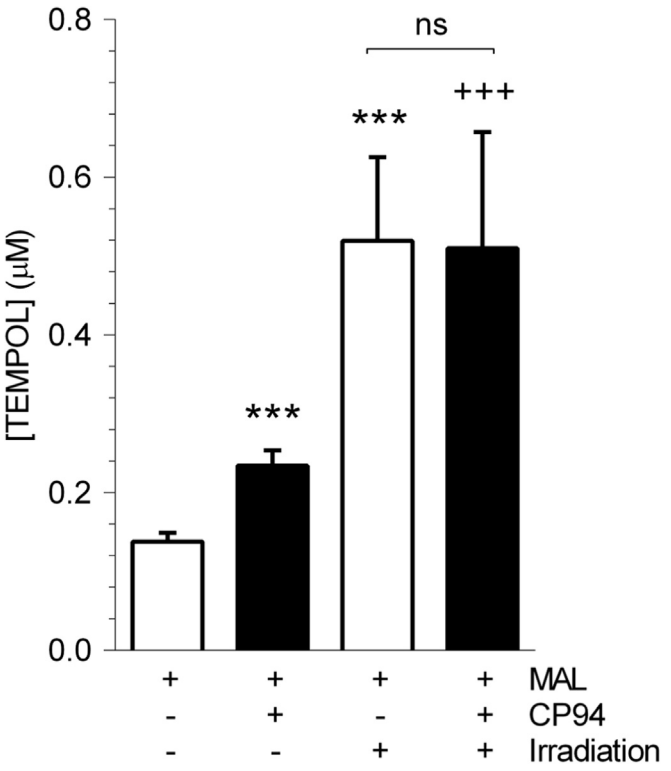

Fig. 7. Concentrations of TEMPOL formed following spin trapping of photodynamically-generated singlet oxygen by TMP in A431 cells. The average peak area of each acquired TEMPOL spectrum was determined and concentrations were established by interpolating values from a standard curve. Interpolated concentrations of TEMPOL formed following spin trapping of photodynamically-generated singlet oxygen by TMP in A431 cells. The average peak area of each acquired TEMPOL spectrum (Fig. 6) was determined and concentrations were established by interpolating values from a standard curve. *** corresponds to $p < 0.001$ (Student's *t*-test) compared to cells treated with MAL only. +++ corresponds to $p < 0.001$ compared to cells treated with MAL and CP94.

concentration of TEMPOL formed prior to irradiation was 1.1 ± 0.3 μM and this increased to 85.0 ± 1.9 μM following irradiation ($p < 0.001$ Student's *t*-test).

Untreated cells did not produce a detectable concentration of the TEMPOL adduct (Fig. 6C). Prior to irradiation, cells treated with MAL produced a small signal, corresponding to a concentration of 0.14 ± 0.01 μM TEMPOL (Fig. 6D). Following irradiation, the signal intensity increased significantly to 0.52 ± 0.11 μM "TEMPOL equivalents" (Fig. 6E, $p < 0.001$ compared to MAL alone). Treatment with MAL and CP94 in the absence of irradiation produced a signal equivalent to 0.23 ± 0.02 μM TEMPOL (Fig. 6F, $p < 0.001$ compared to MAL alone) and irradiation increased this to 0.51 ± 0.15 μM TEMPOL equivalents (Fig. 6G, $p < 0.001$ *compared to* MAL and CP94 dark, $p > 0.05$ compared to treatment with MAL and irradiation). A graphical representation of these values is shown in Fig. 7.

4. Discussion

In the present study, it was observed that CP94 increases the efficacy of MAL-based photodynamic cell killing in a manner associated with an increase in $O_2^{\bullet -}$/ROS, likely localised to the mitochondria. We also report the detection of photo-generated singlet oxygen in whole cells by EPR spectrometry.

It has previously been shown that the treatment of different cell types (including A431 cells) with MAL (0.5 mM) and CP94 (150 μM) significantly increases accumulation of PpIX compared to treating cells with MAL alone [30]. Here, we have shown that CP94 significantly increases PpIX accumulation (3–5 fold) in A431 cells treated with a range of concentrations of MAL.

The type of photosensitiser, localisation of the photosensitiser and the dose of light are all important factors in determining the efficacy of a photodynamic treatment and whether cells will undergo apoptosis or necrosis [3,38,39]. With regard to PpIX-based photodynamic cell killing, it has previously been shown that ALA-induced, mitochondria-localised PpIX was far more efficacious than exogenous, ubiquitously-distributed PpIX when compared at equivalent concentrations [40]. We have previously demonstrated that CP94 significantly increases the efficacy of MAL-based photodynamic cell killing in a range of human cultured cell types, more effectively than the more established iron chelator desferrioxamine [41,42] and is effective with all PpIX congeners (ALA, MAL and HAL (hexaminolevulinate)) and oxygen concentrations (5%, 20% and 40%) investigated to date [43]. Furthermore these experimental findings have translated into greater reductions in tumour thickness when applied to skin cancers clinically [30,31] as CP94 is effective as a topical formulation [44]. Here, we have shown that, following treatment with 0.5 mM MAL and irradiation (25 J/cm^2), A431 cells died primarily by necrosis at each time point measured, with little more than "background" apoptosis. Necrotic cell death was also exhibited by cells treated with MAL and CP94 and irradiation and was found to be significantly higher at each time point compared to treatment without CP94. The high levels of necrosis observed were most likely due to the extensive mitochondrial damage caused by the high concentrations of $^1O_2$ and ROS being generated [45,46]. Furthermore, the significant increase in necrosis caused by CP94 co-treatment at each time point was most likely to be the result of further increases in ROS generation (Fig. 4, discussed below).

The mechanism of action of dermatological PDT is known to be both intricate and complex and clinical success depends on adequate PpIX accumulation throughout the full thickness of the skin lesion to be treated, delivery of the complete light dose at the correct wavelength/time-point in addition to an adequate oxygen supply being available within the treatment area throughout the irradiation period [39]. It is also known that lack of PpIX accumulation in the deeper layers of thicker skin tumours (e.g. nodular basal cell carcinomas) is currently a limiting factor on the clinical effectiveness of dermatological PpIX-induced PDT.

When considered in detail, the exogenous administration of a PpIX precursor manipulates neoplastic cells to synthesise and accumulate PpIX more rapidly than their surrounding normal cells [1]. This innate haem biosynthesis pathway can also be further manipulated through the concurrent administration of the iron chelating agent CP94 to temporarily accumulate elevated amounts of PpIX to enhance the effectiveness of the PDT treatment. However as iron can also play a role in the generation of ROS, limiting its availability through chemical chelation could actually be reducing the efficacy of PpIX-PDT, thus theoretically reducing the maximal PDT effect that is created. Our previous investigations considering this possibility however, have concluded that the positive effects on PDT efficacy produced by increased PpIX accumulation pre-irradiation through the use of the iron chelator CP94, far outweigh any limitations reduced iron availability may have on the ability of iron to catalyse ROS generation/cascades following PpIX-induced PDT [47]. This observation may be explained by alternate transition metals (such as zinc or copper) mediating Fenton-type reactions instead of iron in the subsequent ROS cascades triggered by PpIX-PDT. Additionally, although cellular iron levels are usually tightly regulated under normal circumstances, during oxidative stress iron homeostasis can be disrupted resulting in the release of labile iron [48,49]. So iron chelation with CP94 may initially reduce iron availability increasing PpIX accumulation and

once a state of oxidative stress begins to occur on irradiation, other transition metals and freshly released labile iron may perpetuate the ROS cascades via Fenton reactions [47].

During irradiation, cellular damage is initially caused by the generation of $^1O_2$ and ROS close to the site of PpIX accumulation i.e. the mitochondria [50] and the free radical cascades thus initiated, subsequently transmit the damage throughout the cell generating damage to DNA and other macromolecules [47], which has been observed following PpIX-PDT ± CP94. The initial damage to mitochondrial membranes causes release of cytochrome c and a decrease in cellular ATP. Both of these events occur during and immediately following irradiation and have been shown to initiate apoptosis following PpIX-based photodynamic cell killing in other cell types [51,52]. As time progresses, or if the initial membrane damage is sufficient, a total loss of ATP production occurs, a critical step in the switch from apoptosis to necrosis. If DNA damage occurs, existing ATP can be rapidly depleted by ATP-dependent poly ADP ribose polymerase (PARP) [53]. Depletion of ATP results in decreased activity of ATP-dependent Na^+/K^+ and Ca^{2+} pumps, leading to increased intracellular Na^+ and Ca^{2+}. Excessive intracellular Na^+ and Ca^{2+} leads to osmotic damage [54] and activation of Ca^{2+}-dependent proteases and nucleases [55] associated with necrosis. Here, we found that MAL-based photodynamic cell killing was predominantly necrotic, and that the addition of CP94 to the MAL-based photodynamic system resulted in further increases in necrotic cell death, with little effect on apoptosis.

MnTBAP, a superoxide dismutase mimetic, and L-histidine, a singlet oxygen quencher, were utilised in order to understand the mechanisms of photodynamic cell killing being induced in this system. Both MnTBAP and L-histidine inhibited photodynamic killing in cells treated with MAL, implicating both superoxide and singlet oxygen as key components in the photodynamic process. In cells treated with MAL and CP94, MnTBAP partially inhibited photodynamic cell killing and complete inhibition was achieved by L-histidine.

Considering these results, we propose that in this system, superoxide is produced by the reduction of singlet oxygen, rather than being generated directly by excited-state protoporphyrin IX. Therefore, although superoxide appears to be an important component in the photodynamic process, the generation of singlet oxygen is key to initiate processes that ultimately lead to cell killing.

Post-irradiation, cells treated with MAL exhibited an increased EPR signal intensity in the presence of TEMPOL, indicating $^1O_2$ generation within these cells. As far as we know, this is the first time that PpIX-generated $^1O_2$ has been detected in whole cells by spin trapping with TMP and detection by EPR. A similar TEMPOL signal was also observed post-irradiation in cells treated with MAL and CP94. However, the signal intensity was not significantly different compared to treatment in the absence of CP94. This was unexpected: the measurements of PpIX accumulation and cell death indicated that an increase in $^1O_2$ generation would also be observed, as photosensitiser concentration is thought to be closely linked to the amount of $^1O_2$ generated [56,57], which in turn affects the degree and type of cell death induced [58]. The lack of a detectable difference in TEMPOL signals may be due to an absence of any changes in $^1O_2$ generation, or a limitation of the method used for $^1O_2$ detection in this system, such as a lack of co-localisation of TMP with the photo-generated $^1O_2$ or the competition of TMP with local biomolecules. We have reported (Fig. 6A and B) the formation of high concentrations of $^1O_2$/TMP-derived TEMPOL. However this was under ideal conditions in a cell-free system and it is possible that the detection of intracellular $^1O_2$ may be limited.

The trapping of porphyrin-generated $^1O_2$ by TMP has previously been demonstrated in a cell-free system [59]. The *ex situ* irradiation (λ_{max} 409 nm) of 10 μM porphyrin in the presence of 10 mM TMP resulted in the formation of the $^1O_2$ adduct, TEMPOL. The authors found that the generation of $^1O_2$ was dependent on the light-dose from the irradiation source. This investigation was a good early indication that porphyrins, upon irradiation, could generate $^1O_2$, which in turn could be trapped by TMP in the absence of cells. Similar experiments have been performed with a variety of photosensitisers [9,27,60,61]. However, to our knowledge there has been no documented literature describing the detection of $^1O_2$, by EPR spectrometry, in cells that had been treated with MAL. The results presented here are therefore novel as they are the first to show that $^1O_2$ is generated intracellularly following treatment with MAL-PDT and support the in vivo findings of Laubach et al. who detected $^1O_2$ produced by ALA-PDT conducted on the healthy skin of human volunteers via luminescence [62]. These data strongly indicate that type II photochemical reactions are occurring during the PpIX-based photodynamic treatment.

Our inhibitor studies with MnTBAP indicate that superoxide is being produced in our system and, in PpIX-based PDT, $O_2^{\bullet -}$ and / or $^{\bullet}OH$ are known to be produced directly, as well as indirectly arising from $^1O_2$ [63]. However, there have been very few studies on the production of $O_2^{\bullet -}$ or $^{\bullet}OH$ by PpIX using DEPMPO in conjunction with EPR spectrometry, which could potentially provide a higher degree of specificity compared to previously used methods. The DEPMPO-OOH adduct signal was not detected in our system. This is potentially due to a low concentration of $O_2^{\bullet -}$ production, compared to $^1O_2$, which may be below the limit of detection. This may be further exacerbated by localisation issues, whereby DEPMPO does not co-localise with mitochondria-localised PpIX in sufficient quantities to produce a detectable signal.

Porphyrin-based photosensitisers have previously been shown to generate $O_2^{\bullet -}$ and $^{\bullet}OH$ in a cell-free system [64]. Irradiation of hematoporphyrin, in the presence of DMPO and DTPA resulted in the formation of the DMPO-OH adduct. Addition of superoxide dismutase (SOD) significantly decreased the DMPO-OH signal, indicating that $O_2^{\bullet -}$ was being generated, but as the DMPO-OOH adduct was not detected it was suggested that $O_2^{\bullet -}$ was rapidly decaying to $^{\bullet}OH$ in this system. The addition of catalase did not have an effect on the signal intensity, ruling out the role of H_2O_2 with this type of photosensitiser [64]. However it has previously been demonstrated in vivo with ALA-induced PpIX-PDT that both the combination of SOD with catalase or alternatively allopurinol (an inhibitor of xanthine oxidase) administration, protected against PDT-induced tissue damage [65]. This indicated that reperfusion injury was implicated in the mechanism of action in this experimental model, a finding further endorsed by clinical observations of oxygen saturation, perfusion data and PpIX fluorescence changes in human skin cancers and pre-cancers [39]. It is therefore likely that on irradiation, singlet oxygen and other ROS are rapidly produced via photochemical reactions, reducing oxygen and ground state PpIX availability (via photochemical consumption and singlet oxygen destruction respectively). The rapid oxygen consumption could initiate hypoxia and subsequently trigger hypoxia-induced vasodilation, leading to increased perfusion and an accompanying replenishment (or partial replenishment) of the depleted oxygen supply. Nevertheless, oxygen will continue to be consumed as long as adequate ground state PpIX remains to “feed” the cell-damaging PDT reactions [39].

To detect ROS generated by photo-irradiated PpIX, DHE and its mitochondria-targeted derivative MitoSOX were utilised. The use of fluorogenic probes sacrifices specificity in exchange for superior sensitivity compared to EPR spectrometry. DHE was chosen for this study as it is known that the hydroxylated ethidium analogue formed is $O_2^{\bullet -}$-specific (2-hydroxy ethidium; 2-OH-E^+). An additional advantage of using DHE is that the mitochondria-targeted derivative, MitoSOX, is available, allowing the detection of

wholecell ROS versus mitochondrial ROS generation using the same detection system. It has previously been shown that the reaction of DHE and MitoSOX with $O_2^{\bullet -}$ both yield their corresponding 2-OH-E^+ analogues [66]. In the present system, it is not instructive to compare the fluorescence intensities of DHE and MitoSOX directly, as (a) they accumulate to different extents depending on membrane potentials [15] and (b) different concentrations have been used. However, we can draw some conclusions based on their relative fluorescence compared to their respective untreated controls. Treatment with MAL and irradiation led to a significant increase in DHE and MitoSOX-derived 2-OH-E^+ fluorescence. Furthermore, compared to their respective untreated controls, the MitoSOX-derived fluorescence was observed to be significantly higher when compared to that of DHE, potentially indicating a higher concentration of mitochondria-localised $O_2^{\bullet -}$, compared to that present within the cytosol. The addition of CP94 to the treatment resulted in further increases in both DHE and MitoSOX fluorescence. Again, compared to their respective untreated controls, the increase in MitoSOX fluorescence intensity was significantly higher than that of DHE, , which is suggestive of a larger increase in mitochondria-localised ROS, including $O_2^{\bullet -}$. The addition of MnTBAP, a known superoxide dismutase-mimetic, decreased the production of DHE and MitoSOX-derived 2-OH-E^+, providing further evidence that $O_2^{\bullet -}$ was detected in this system.

As the accumulation of MitoSOX within the mitochondria is dependent on the mitochondrial membrane potential, it is clear that treatments which disrupt the function of mitochondria may have an effect on the localising capability of MitoSOX. Nevertheless, MitoSOX has been widely used as a detector of mitochondrial ROS under conditions where the mitochondrial membrane potential is known to be affected: for example, the complex I inhibitor rotenone has been shown to decrease mitochondrial membrane potential [67,68] whilst simultaneously increasing the generation of mitochondria-localised $O_2^{\bullet -}$ [69] as measured by MitoSOX [70] and other methods [71,72]. As the irradiation in our system was carried out following pre-treatment with MitoSOX, the MitoSOX would be present within the mitochondrial matrix at the commencement of irradiation [73] and, if the mitochondrial membrane potential subsequently decreased enough to affect the localisation of MitoSOX, we would expect to see results similar to those obtained with DHE. With this in mind, we believe that our experiments with MitoSOX tell us that the source of these ROS is likely to be mitochondrial in nature.

The use of DHE to detect ROS in PpIX-based photodynamic cell killing of A431 cells has previously been described [74]. Cells were treated with ALA (1 mM) for 8 h, after which they were irradiated with a range of light doses (0–45 J/cm^2, λ_{max} 630 nm). Detection of the fluorescent product was carried out by flow cytometry, with excitation at 488 nm and emission detection at 600 ± 20 nm. The authors reported a light-dose- dependent production of $O_2^{\bullet -}$, up to the highest tested dose of 45 J/cm^2.. In the absence of ALA, irradiation did not result in the formation of any fluorescent product at any light dose. Additionally, the generation of $O_2^{\bullet -}$ correlated with cell death, measured 30 min post-irradiation by propidium iodide staining in conjunction with flow cytometry. Even though DHE was used to determine the production of "$O_2^{\bullet -}$", at the time of this work being carried out it was not yet known that two fluorescent products were formed and it is likely that carrying out the detection using the method described would have resulted in the detection of fluorescence from both the E^+ and 2-OH-E^+. However, the observation that cell death and ROS/$O_2^{\bullet -}$ generation are correlated, agrees with the results presented here.

In conclusion, these data indicate that, under the conditions described here, human skin cancer cells treated with MAL-based photodynamic cell killing in the absence and presence of the iron chelating agent CP94 die in a predominantly necrotic manner. Furthermore, the degree of cell death appears to be, in part, dependent on the amount of mitochondria-localised ROS generated during photoirradiation. $O_2^{\bullet -}$ may play a key role in the outcome of PpIX-based photodynamic treatments and CP94-induced increases in efficacy may be partly due to an increase in mitochondria-localised $O_2^{\bullet -}$ generation.

Contributions

YD designed and performed experiments, analysed data, and drafted and revised the paper. DCJF designed and performed experiments, analysed data, and drafted and revised the paper. ND contributed to the design of some experiments, interpretation of the results and the revision of the paper. AC co-conceived the project, contributed to the design of some experiments, interpretation of results, co-supervised YD & DCJF and revised the draft paper. GS contributed to the design of some experiments, interpretation of results, co-supervised DCJF and revised the draft paper. PGW co-conceived the project, designed and monitored the execution of all experiments, analysed and interpreted data, co-supervised YD & DCJF and revised the draft paper.

Acknowledgements

We thank Professor Robert Hider, King's College London, for providing the iron chelating agent (CP94), and Drs Paul Eggleton and Jo Tarr (University of Exeter Medical School) for their assistance with the flow cytometry analysis. The Duchy Health Charity Ltd (DCH05-07), Peninsula Medical School and DDRC Healthcare (GD100015-122) are thanked for financial support. PGW and DCJF acknowledge financial support from the European Cooperation in Science and Technology, Belgium (COST Action BM1203/EU-ROS).

References

[1] Q. Peng, et al., 5-Aminolevulinic acid-based PDT: principles and experimental research, Photochem. Photobiol. 65 (2) (1997) 235–251.
[2] A. Castano, Mechanisms in photodynamic therapy: part one – photosensitizers, photochemistry and cellular localization, Photo. Photodyn. Ther. 1 (2004) 279–293.
[3] N.L. Oleinick, H.H. Evans, The photobiology of photodynamic therapy: cellular targets and mechanisms, Radiat. Res. 150 (5 Suppl) (1998) S146–S156.
[4] C.H. Morton, et al., Guidelines for topical photodynamic therapy: report of a workshop of the British Photodermatology Group, Br. J. Dermatol. 146 (2002) 552–567.
[5] Q. Peng, et al., 5-Aminolevulinic acid-based photodynamic therapy. Clinical research and future challenges, Cancer 79 (12) (1997) 2282–2308.
[6] S.W. Ryter, R.M. Tyrrell, Singlet molecular oxygen ((1)O2): a possible effector of eukaryotic gene expression, Free Radic. Biol. Med. 24 (9) (1998) 1520–1534.
[7] A.P. Castano, T.N. Demidova, M.R. Hamblin, Mechanisms in photodynamic therapy: part one–photosensitizers, photochemistry and cellular localization, Photo. Photodyn. Ther. 1 (4) (2004) 279.
[8] R.F.V. Lopez, et al., Photodynamic therapy of skin cancer: controlled drug delivery of 5-ALA and its esters, Adv. Drug Deliv. Rev. 56 (1) (2004) 77–94.
[9] Z. Lu, et al., Mitochondrial reactive oxygen species and nitric oxide-mediated cancer cell apoptosis in 2-butylamino – 2-demethoxyhypocrellin B photodynamic treatment, Free Radic. Biol. Med. 41 (10) (2006) 1590–1605.
[10] K. Plaetzer, et al., The modes of cell death induced by PDT: an overview, Med. Laser Appl. 18 (2003) 7–19.
[11] K. Plaetzer, et al., Apoptosis following photodynamic tumor therapy: induction, mechanisms and detection, Curr. Pharm. Des. 11 (9) (2005) 1151–1165.
[12] K. Plaetzer, et al., Photophysics and photochemistry of photodynamic therapy: fundamental aspects, Lasers Med Sci. 24 (2) (2009) 259–268.
[13] B. Halliwell, M. Whiteman, Measuring reactive species and oxidative damage in vivo and in cell culture: how should you do it and what do the results mean? Br. J. Pharmacol. 142 (2) (2004) 231–255.
[14] B. Kalyanaraman, et al., Measuring reactive oxygen and nitrogen species with fluorescent probes: challenges and limitations, Free Radic. Biol. Med. 52 (1) (2012) 1–6.
[15] K.M. Robinson, et al., Selective fluorescent imaging of superoxide in vivo using ethidium-based probes, Proc. Natl. Acad. Sci. USA 103 (41) (2006)

15038–15043.
[16] P.G. Winyard, et al., Determination of S-nitrosothiols in biological and clinical samples using electron paramagnetic resonance spectrometry with spin trapping, Methods Enzym. 441 (2008) 151–160.
[17] N.J.F. Dodd, A.N. Jha, Photoexcitation of aqueous suspensions of titanium dioxide nanoparticles: an electron spin resonance spin trapping study of potentially oxidative reactions, Photochem. Photobiol. 87 (3) (2011) 632–640.
[18] A.K. Haylett, et al., Singlet oxygen and superoxide characteristics of a series of novel asymmetric photosensitizers, Cancer Lett. 112 (2) (1997) 233–238.
[19] J.F. Reeves, et al., Hydroxyl radicals ((OH)-O-center dot) are associated with titanium dioxide (TiO_2) nanoparticle-induced cytotoxicity and oxidative DNA damage in fish cells, Mutat. Res. -Fundam. Mol. Mech. Mutagen. 640 (1–2) (2008) 113–122.
[20] N. Khan, et al., Spin traps: in vitro toxicity and stability of radical adducts, Free Radic. Biol. Med. 34 (11) (2003) 1473–1481.
[21] H. Shi, et al., Evaluation of spin trapping agents and trapping conditions for detection of cell-generated reactive oxygen species, Arch. Biochem. Biophys. 437 (1) (2005) 59–63.
[22] J. Moan, E. Wold, Detection of singlet oxygen production by ESR, Nature 279 (5712) (1979) 450–451.
[23] C. Hadjur, et al., Production of the free radicals O.-2 and .OH by irradiation of the photosensitizer zinc(II) phthalocyanine, J. Photochem. Photobiol. B: Biol. 38 (2–3) (1997) 196–202.
[24] C.F. Chignell, Spin trapping studies of photochemical reactions, Pure Appl. Chem. 62 (1990) 301–305.
[25] J.X. Pan, et al., Photodynamic action of actinomycin D: an EPR spin trapping study, Biochim. Biophys. Acta 1527 (1–2) (2001) 1–3.
[26] Y. Tokuoka, et al., ESR spectroscopy of singlet oxygen generated by protoporphyrin IX in aqueous surfactant solutions, J Oleo Sci. 52 (3) (2003) 135–140.
[27] T. Wu, et al., Photodynamic action of amino substituted hypocrellins: EPR studies on the photogenerations of active oxygen and free radical species, J. Photochem. Photobiol. B: Biol. 57 (1) (2000) 14–21.
[28] A. Curnow et al., Using iron chelating agents to enhance dermatological PDT, in: Proceedings the 12th World Congress of the International Photodynamic Association: Photodynamic Therapy: Back to the Future, 2009, 7380.
[29] A. Curnow, et al., Enhancement of 5-aminolaevulinic acid-induced photodynamic therapy in normal rat colon using hydroxypyridinone iron-chelating agents, Br. J. Cancer 78 (10) (1998) 1278–1282.
[30] A. Pye, S. Campbell, A. Curnow, Enhancement of methyl-aminolevulinate photodynamic therapy by iron chelation with CP94: an in vitro investigation and clinical dose-escalating safety study for the treatment of nodular basal cell carcinoma, J. Cancer Res. Clin. Oncol. 134 (8) (2008) 841–849.
[31] S.M. Campbell, et al., Clinical investigation of the novel iron-chelating agent, CP94, to enhance topical photodynamic therapy of nodular basal cell carcinoma, Br. J. Dermatol. 159 (2) (2008) 387–393.
[32] N.O. Karpinich, et al., The course of etoposide-induced apoptosis from damage to DNA and p53 activation to mitochondrial release of cytochrome c, J. Biol. Chem. 277 (19) (2002) 16547–16552.
[33] H. Lundqvist, et al., Phorbol myristate acetate-induced NADPH oxidase activity in human neutrophils: only half the story has been told, J. Leukoc. Biol. 59 (2) (1996) 270–279.
[34] J.R. Geffner, et al., Neutrophil erythrotoxicity induced by phorbol myristate acetate: mechanisms involved in neutrophil activation, J. Leukoc. Biol. 49 (4) (1991) 352–359.
[35] V. Roubaud, et al., Quantitative measurement of superoxide generation and oxygen consumption from leukocytes using electron paramagnetic resonance spectroscopy, Anal. Biochem. 257 (2) (1998) 210–217.
[36] V. Brezová, et al., EPR study of photochemical transformations of triarylmethane dyes, Dyes Pigment. 61 (2) (2004) 177–198.
[37] S. Suy, et al., Nitroxides Tempol and tempo induce divergent signal transduction pathways in MDA-MB 231 breast cancer cells, J. Biol. Chem. 273 (28) (1998) 17871–17878.
[38] D. Kessel, Y. Luo, Mitochondrial photodamage and PDT-induced apoptosis, J. Photochem. Photobiol. B 42 (2) (1998) 89–95.
[39] A. Curnow, J. Tyrrell, The Mechanism of Action of Topical Dermatological Photodynamic Therapy. Photodynamic Therapy: Fundamentals, Applications and Health Outcomes, New York, 2015, p. 43.
[40] Z. Ji, et al., Subcellular localization pattern of protoporphyrin IX is an important determinant for its photodynamic efficiency of human carcinoma and normal cell lines, J. Photochem. Photobiol. B 84 (3) (2006) 213–220.
[41] A. Curnow, A. Pye, Biochemical manipulation via iron chelation to enhance porphyrin production from porphyrin precursors, J. Environ. Pathol. Toxicol. Oncol. 26 (2) (2007) 89–103.
[42] A. Pye, A. Curnow, Direct comparison of delta-aminolevulinic acid and methyl-aminolevulinate-derived protoporphyrin IX accumulations potentiated by desferrioxamine or the novel hydroxypyridinone iron chelator CP94 in cultured human cells, Photochem. Photobiol. 83 (3) (2007) 766–773.
[43] E. Blake, J. Allen, A. Curnow, The effects of protoporphyrin IX-induced photodynamic therapy with and without iron chelation on human squamous carcinoma cells cultured under normoxic, hypoxic and hyperoxic conditions, Photo. Photodyn. Ther. 10 (4) (2013) 575–582.
[44] A. Curnow, A.J. MacRobert, S.G. Bown, Enhancing protoporphyrin IX-induced photodynamic therapy with a topical iron chelating agent in a normal skin model, J. Heavy Metal. Chelation Ther. 1 (2015) 1–9.
[45] R.D. Almeida, et al., Intracellular signaling mechanisms in photodynamic therapy, Biochim Biophys. Acta 1704 (2) (2004) 59–86.
[46] W. Fiers, et al., More than one way to die: apoptosis, necrosis and reactive oxygen damage, Oncogene 18 (54) (1999) 7719–7730.
[47] A. Curnow, A. Pye, The importance of iron chelation and iron availability during PpIX-induced photodynamic therapy, Photonics Lasers Med. 4 (2015) 39–58.
[48] J.L. Zhong, et al., Susceptibility of skin cells to UVA-induced necrotic cell death reflects the intracellular level of labile iron, J. Investig. Dermatol. 123 (4) (2004) 771–780.
[49] A. Pye, et al., Photodynamic therapy with aminolaevulinic acid and iron chelators: a clinical example of redox signaling, in: C. Jacob, P. Winyard (Eds.), Redox Signaling and Regulation in Biology and Medicine, Wiley-VCH, Weinheim, 2009, pp. 381–404.
[50] M. Niedre, M.S. Patterson, B.C. Wilson, Direct near-infrared luminescence detection of singlet oxygen generated by photodynamic therapy in cells in vitro and tissues in vivo, Photochem. Photobiol. 75 (4) (2002) 382–391.
[51] T. Kriska, W. Korytowski, A.W. Girotti, Role of mitochondrial cardiolipin peroxidation in apoptotic photokilling of 5-aminolevulinate-treated tumor cells, Arch. Biochem. Biophys. 433 (2) (2005) 435–446.
[52] D. Grebenova, et al., Mitochondrial and endoplasmic reticulum stress-induced apoptotic pathways are activated by 5-aminolevulinic acid-based photodynamic therapy in HL60 leukemia cells, J. Photochem. Photobiol. B 69 (2) (2003) 71–85.
[53] H.C. Ha, S.H. Snyder, Poly(ADP-ribose) polymerase is a mediator of necrotic cell death by ATP depletion, Proc. Natl. Acad. Sci. USA 96 (24) (1999) 13978–13982.
[54] A.H. Wyllie, E. Duvall, Cell injury and death, in: J. McGee, P.G. Isaacson, N. A. Wright (Eds.), Volume 1 Principals of Pathology, Oxford University Press, Oxford, 1992, pp. 143–240.
[55] J. Bruce, Plasma membrane calcium pump regulation by metabolic stress. World, J. Biol. Chem. 1 (7) (2010) 221–228.
[56] M. Price, L. Heilbrun, D. Kessel, Effects of the oxygenation level on formation of different reactive oxygen species during photodynamic therapy, Photochem. Photobiol. 89 (3) (2013) 683–686.
[57] M. Price, et al., Monitoring singlet oxygen and hydroxyl radical formation with fluorescent probes during photodynamic therapy, Photochem. Photobiol. 85 (5) (2009) 1177–1181.
[58] J. Berlanda, et al., Comparative in vitro study on the characteristics of different photosensitizers employed in PDT, J. Photochem. Photobiol. B-Biol. 100 (3) (2010) 173–180.
[59] S. Cannistraro, P.L. Indovina, Electron spin resonance of serum metallo-proteins in myocardial infarction, Phys. Med. Biol. 24 (1) (1979) 198–199.
[60] K. Ishii, et al., In vitro photodynamic effects of phthalocyaninatosilicon covalently linked to 2,2,6,6-tetramethyl-1-piperidinyloxy radicals on cancer cells, Free Radic. Biol. Med. 38 (7) (2005) 920–927.
[61] S. Xu, et al., Butylamino-demethoxy-hypocrellins and photodynamic therapy decreases human cancer in vitro and in vivo, Biochim. Biophys. Acta 1537 (3) (2001) 222–232.
[62] H.J. Laubach, et al., In-vivo singlet oxygen dosimetry of clinical 5-aminolevulinic acid photodynamic therapy, J. Biomed. Opt. 13 (5) (2008).
[63] F.S. De Rosa, M.V. Bentley, Photodynamic therapy of skin cancers: sensitizers, clinical studies and future directives, Pharm. Res. 17 (12) (2000) 1447–1455.
[64] G.R. Buettner, L.W. Oberley, The apparent production of superoxide and hydroxyl radicals by hematoporphyrin and light as seen by spin-trapping, FEBS Lett. 121 (1) (1980) 161–164.
[65] A. Curnow, S.G. Bown, The role of reperfusion injury in photodynamic therapy with 5-aminolaevulinic acid–a study on normal rat colon, Br. J. Cancer 86 (6) (2002) 989–992.
[66] J. Zielonka, et al., Cytochrome c-mediated oxidation of hydroethidine and mito-hydroethidine in mitochondria: identification of homo- and heterodimers, Free Radic. Biol. Med 44 (5) (2008) 835–846.
[67] C. Chauvin, et al., Rotenone inhibits the mitochondrial permeability transition-induced cell death in U937 and KB cells, J. Biol. Chem. 276 (44) (2001) 41394–41398.
[68] A. Barrientos, C.T. Moraes, Titrating the effects of mitochondrial complex I impairment in the cell physiology, J. Biol. Chem. 274 (23) (1999) 16188–16197.
[69] J.F. Turrens, Mitochondrial formation of reactive oxygen species, J. Physiol. 552 (Pt 2) (2003) 335–344.
[70] K.K. Lee, et al., Isoniazid-induced cell death is precipitated by underlying mitochondrial complex I dysfunction in mouse hepatocytes, Free Radic. Biol. Med 65 (2013) 584–594.
[71] S.I. Dikalov, et al., EPR detection of cellular and mitochondrial superoxide using cyclic hydroxylamines, Free Radic. Res 45 (4) (2011) 417–430.
[72] N. Li, et al., Mitochondrial complex I inhibitor rotenone induces apoptosis through enhancing mitochondrial reactive oxygen species production, J. Biol. Chem. 278 (10) (2003) 8516–8525.
[73] M.P. Murphy, Targeting lipophilic cations to mitochondria, Biochim Biophys. Acta 1777 (7–8) (2008) 1028–1031.
[74] Y. Gilaberte, et al., Flow cytometry study of the role of superoxide anion and hydrogen peroxide in cellular photodestruction with 5-aminolevulinic acid-induced protoporphyrin IX, Photodermatol. Photoimmunol. Photomed. 13 (1–2) (1997) 43–49.